Journal of Macromolecular Science, Part A
Publication details, including instructions for authors and subscription information:
http://www.informaworld.com/smpp/title~content=t713597274

Failure Processes in Fiber-Reinforced Liquid-Crystalline Polyester Composites

T. Weng[a]; A. Hiltner[a]; E. Baer[a]
[a] Department of Macromolecular Science, Case Institute of Technology Case Western Reserve University, Cleveland, Ohio

To cite this Article Weng, T. , Hiltner, A. and Baer, E.(1989) 'Failure Processes in Fiber-Reinforced Liquid-Crystalline Polyester Composites', Journal of Macromolecular Science, Part A, 26: 1, 273 — 307
To link to this Article: DOI: 10.1080/00222338908053852
URL: http://dx.doi.org/10.1080/00222338908053852

J. MACROMOL. SCI.–CHEM., A26(1), pp. 273-307 (1989)

FAILURE PROCESSES IN FIBER-REINFORCED LIQUID-CRYSTALLINE POLYESTER COMPOSITES

T. WENG, A. HILTNER, and E. BAER

Department of Macromolecular Science
Case Institute of Technology
Case Western Reserve University
Cleveland, Ohio 44106

ABSTRACT

A hierarchical structural model for liquid-crystalline polyester reinforced with short glass fibers has been determined by using injection-molded bars. The gradient structure showed similar orientations between the glass fibers and the molecular orientation of the matrix. In the fiber-reinforced composites, the core failed prior to the skin by matrix cracking and transverse fiber pull-out as evidenced by the initial growth of parabolic cracks in the core. In the 30 wt% composite this was followed by complex cooperative phenomena involving fiber breakage, debonding, pull-out, and matrix deformation in the skin. The 50 wt% composite failed prematurely due to inadequate fiber/matrix interactions in the skin structure. Acoustic emission coupled with microscopy provided mechanistic insight throughout this work into the amount and intensity of specific failure mechanisms.

INTRODUCTION

Short-fiber-reinforced thermoplastics and thermosets are of great technological importance as engineering materials. Due to their high moduli, high specific strength, and superior physical properties compared to their unreinforced counterparts, they have been extensively used in many commer-

cial applications. The mechanical behavior of these composites is highly dependent on the fiber type, length, volume fraction, and orientation as well as the interfacial shear strength [1]. Furthermore, the type of matrix used is an important factor for the fracture toughness and fatigue properties of these composites. Most of the research and commercial developments to date have been focused on the more conventional flexible chain resin types. With the recent advances in the field of the thermotropic liquid-crystalline polyesters [2], new opportunities for their applications as matrix materials with carbon and glass fibers are being explored.

Few studies have been published on the injection-molded liquid-crystalline polyesters in either the unreinforced or the reinforced state. For the unreinforced state, Jackson and Kuhfuss [3] were first to report highly anisotropic properties in injection-molded parts of *p*-hydroxybenzoic (PHB) and poly(ethylene terephthalate) (PET) copolyesters, later known as X-7G. McFarlane et al. [4] reported similar results on copolyesters of different moieties. The mechanical and physical properties of a thermotropic terpolymer system under various molding conditions were discussed by Ophir and Ide [5]. They reported the presence of a layer-like structure resulting from complex flows during mold filling. Similar observations were also made on X-7G polymer when subjected to different types of flow histories [6]. Thapar and Bevis concluded from etching techniques that the sheet-like structures seen in the scanning electron microscope consisted of nodulated fibrils of different sizes [7].

In a more detailed study on the morphology of injection-molded parts, Weng et al. [8] elucidated the gradient solid-state structure of the layers. A hierarchical structural model describing at least four levels of organizations was proposed. Similar hierarchical structural models observed in fibers, extrudates, and injection-molded articles have also been proposed by Sawyer and Jaffe [9]. Their proposed models were based on a broad range of thermotropic polyester compositions. Baird and Wilkes [10] investigated the feasibility of sandwich injection molding copolymers of PHB/PET with filled PET for the reinforced state. Voss and Friedrich [11] found poor enhancement in the mechanical properties when short glass and carbon fibers were added to a liquid-crystalline polymer matrix. This was attributed to weak interfacial adhesion between the matrix and the fibers.

It is the purpose of this work to determine the morphology of injection-molded thermotropic liquid-crystalline polyesters reinforced with short glass fibers and to characterize the microfailure processes and fracture during deformation. Acoustic emission AE has been used extensively for fibrous composite materials in the last two decades. The technique is based on a phenomenon requiring sudden release of strain energy, which commonly occurs

in composite materials under damaging external stresses. The most common methods of analysis are by frequency [12] and by amplitude distribution. In amplitude distribution analysis, which is the method employed in this study, the amplitude peaks are usually associated with the different microfailure processes observed during deformation. Mehan and Mullin [13] indicated that there are basically three main failure mechanisms in fibrous composites: matrix cracking, interfacial debonding, and fiber fracture, these being arranged in the order of ascending energies and consequently of higher amplitudes. Various investigators [14-20] have confirmed the above suggested correlation between the amplitude and the nature of the failure processes. On the other hand, others have indicated that the high amplitude peaks corresponded to matrix cracking and not necessarily to fiber breakage [21-24].

Despite some discrepancy in the literature on assigning the low- and high-amplitude events to the precise nature of damage in composites, it is very likely that the proposed modes of failure are only valid for the particular matrix/filler composite system investigated. Acoustic emission cannot be considered as a "standalone" tool, but must be supported by other techniques to provide additional information. Consequently, in this study, optical and scanning electron microscopy were used as complementary techniques to characterize the microfailure processes during deformation.

EXPERIMENTAL

Materials

The neat resin material used in this study was a thermotropic liquid-crystalline polyester commercialized by Celanese Corp. under the trade name Vectra A950. Two loadings of short glass fibers were investigated: 30 and 50 wt%. Samples were kindly supplied by the Celanese Research Corp., Summit, New Jersey, in the form of injection-molded bars having the dimensions; 127 X 12.7 X 3.2 mm. The molding conditions were as follows: melt temperature 300°C, mold temperature 100°C. Additional information regarding the chemical composition of the resin, the type and size of the glass fibers, the coupling agent used, if any, was not revealed by the manufacturer.

Mechanical Measurements

Stress-strain measurements were conducted on an Instron mechanical testing machine Model 1123. Test specimens were cut into a tensile "dog-bone"

geometry from a molded bar. At least 5-10 samples were tested in the acoustic emission measurements. The strain rate used was 1%/min.

Optical Microscopy (OM)

Two types of microscopes were employed in this study. A Nikon polarizing optical microscope attached to a motor-driven 35mm camera was used in conjunction with the Instron machine and the acoustic emission instrument to observe the deformation processes simultaneously. Photographs were taken at regular time intervals corresponding to specific strains and analyzed with the detected acoustic emission signals. An Olympus optical microscope Model BHM was used in a static mode to determine the orientation of the glass fibers in the composite materials. Samples were cut at different cross sections with respect to the mold-filling direction (MFD). The surfaces were further polished by conventional metallographic techniques and observed in the reflection mode of the microscope by using a differential interference contrast method, the Nomarski method, to enhance the contrast and relief of the images.

Scanning Electron Microscopy (SEM)

Fracture surfaces of the composite materials were examined by a JEOL scanning electron microscope (SEM) Model TSM-35CF. The SEM was also used to observe *in situ* the microdeformation processes in the composites by means of a mini 3-point bend setup as described by Sato et al. [25]. The observation was focused on the tensile side of the sample which was polished with alumina powders of different particle sizes before being coated with gold/palladium. The same procedure of observing the microfailure processes was applied in tension instead of 3-point bending. The procedure consisted of stretching a tensile specimen outside the SEM chamber at different predetermined strains, followed by observation in the microscope after each stretch. Both the 3-point bending and tensile tests gave similar results.

Wide-Angle X-Ray Measurements (WAXS)

In order to determine the preferred molecular orientation in the resin material and to draw a qualitative comparison with the orientation of the glass fibers in the composite systems, wide-angle x-ray measurements were performed on samples microtomed from different depths from the surface of the molded bar. The microtoming, which yielded slices of approximately 15 μm in thickness, was done by a tungsten-carbide knife in a heavy-duty

microtome K apparatus. X-ray diffraction patterns were obtained with a Searle toroidal focusing camera and nickel-filtered CuK_α radiation.

Acoustic Emission (AE)

A differential wide-band transducer with an almost flat frequency response over 10-1000 kHz was used to monitor the acoustic emission signals during tension. The transducer, which was a piezoelectric crystal PZT, was held firmly against the surface of the tensile specimen by a rubber band with vacuum grease as a coupling medium. The signals detected were first preamplified at a fixed gain of 40 dB through a low-noise preamplifier Model 1220A. The signals were further filtered before being amplified again through the main amplifier at 20 dB. The analysis and evaluation of the signals were done on a Physical Acoustic Corp. PAC 3000/3004 system. To eliminate the noise coming from the mechanical grips of the Instron machine, the so-called "guard sensors" were activated. These were placed equidistantly from the main sensor close to the griping device. The threshold level was set at 25 dB and a 40-μs dead time was chosen for data acquisition.

RESULTS AND DISCUSSION

Hierarchical Structure of LCP Composites

The hierarchical structure previously postulated for an injection-molded plaque of a similar LCP matrix material is shown in Fig. 1(a). This type of morphology with a strong gradient structure has been discussed in detail elsewhere [8]. As previously noted, the top layer is highly oriented into a fibrillar structure. Underneath this layer, the structure changes to a layered morphology composed of sublayers and microlayers which are interconnected with microfibers. The core is relatively featureless and reflects only the localized flow pattern.

The corresponding hierarchical model for the short-glass-fiber-reinforced LCP composites is sketched in Fig. 1(b). This simplified descriptive model is based on optical micrographs taken from cross sections parallel and perpendicular to the mold-filling direction, MFD. Figure 2 shows the orientation of the glass fibers in the composites. These results show similar features to the neat injection-molded material. That is, two skin macrolayers are observed in which the fibers are mostly oriented parallel to the MFD and a core macrolayer where, as previously noticed, the fibers reflect the flow field. Consequently, the fibers are partially aligned perpendicular to the flow direction.

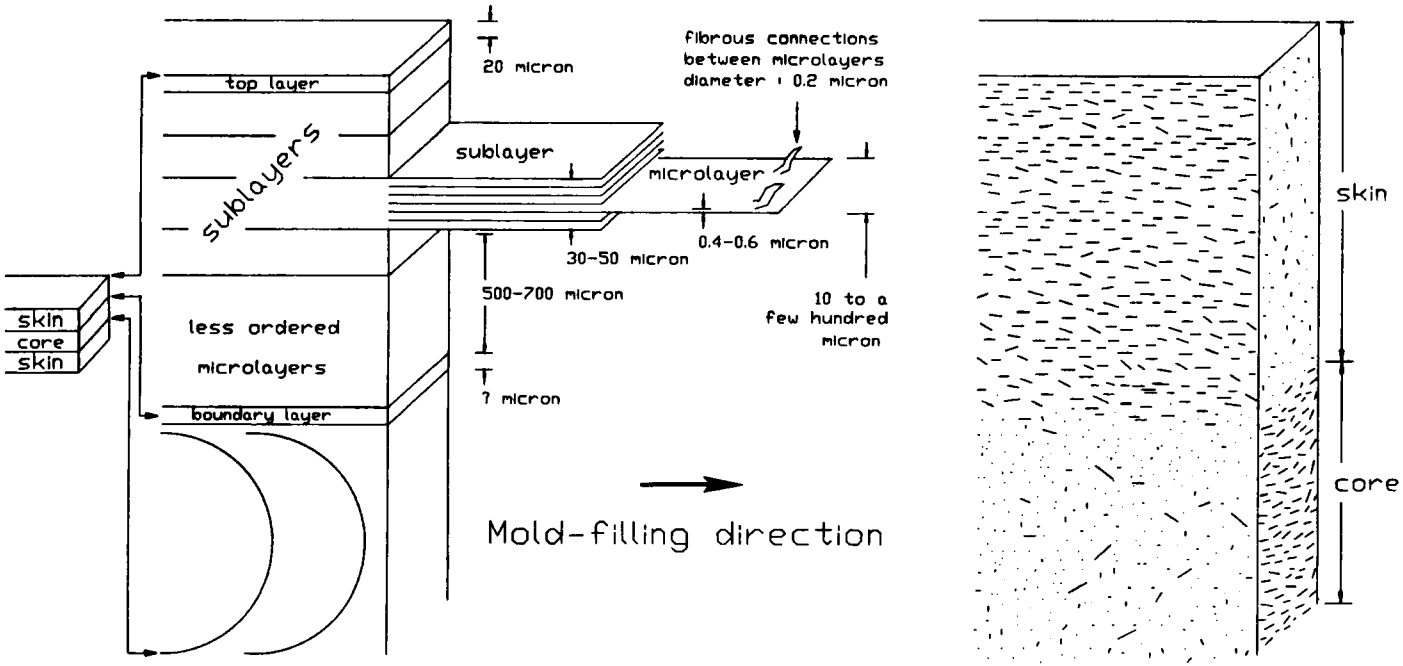

a. LCP matrix **b. LCP composite**

FIG. 1. Proposed hierarchical model of injection-molded (a) unreinforced LCP resin material and (b) its short-fiber-reinforced composite.

A new more detailed view is obtained by observing cross sections cut parallel to the surface at different depths of the mold. Figures 3, 4, and 5 show the orientation of the fibers at the surface, at 0.2 thickness ($0.2t$) away from the surface, and at the center ($0.5t$), respectively. It is quite evident from the OM examinations of the composite systems shown in Figs. 3(b) and 3(c) that the glass fibers at the surface are highly oriented along the MFD. Also, the degree of orientation decreases gradually as one proceeds inward into the mold, as shown in Figs. 4(b) and 4(c). The WAXS patterns given in Figs. 3(a) and 4(a), which result from the LCP resin only, suggest a similar macromolecular orientation at corresponding distances from the surface of the mold. In this gradient structure the degree of preferred molecular orientation was found to be high in the top layer and decreased gradually as one proceeds into the sublayers. In the core the expected similarity in the orientation with the neat injection-molded resin is again observed. Correspondingly, fiber alignment into the parabolic flow pattern from the longitudinal cross sections parallel to the MFD is shown in Figs. 2(a) and 2(b) and in the "in-plane" cross sections parallel to the surface in Figs. 5(b) and 5(c).

These types of orientational phenomena seen in the neat LCP resin material and in its corresponding short-glass-fiber composites are similar to the characteristics of many short-fiber-reinforced thermoplastics and thermosets [26-33]. A quantitative description of the rheological variables during the injection molding that control the development of such layered structures with distinct fiber orientation has not been achieved. A semiquantitative model has been proposed for the injection molding of unreinforced amorphous polymers [34]. Several investigators have indicated that the predominant mechanism which gives rise to fiber orientation is due to elongational flow [26, 35-37]. Kenig attributed the development of fiber orientation to four main types of flow: elongational flow, shear flow, converging flow, and spreading radial flow [37]. By applying these flow mechanisms to injection-molded short-fiber-reinforced composites, the elongational flow contributes mainly to the high degree of orientation in the surface along the MFD. While converging flow also leads to some alignment in the MFD, shear flow is predominantly responsible for fiber orientation in the flow direction at some distance away from the surface. Conversely, fiber orientation in the transverse direction can be attributed to spreading radial flow, which indicates that the glass fibers in the core should be oriented perpendicular to the MFD.

It is quite reasonable to suggest the evolution of the gradient hierarchical structure in the LCP systems results from these complex flow mechanisms. Shear and elongational flows presumably are the cause for the longitudinal gradient structure in the skin macrolayer, while the transverse orientation in

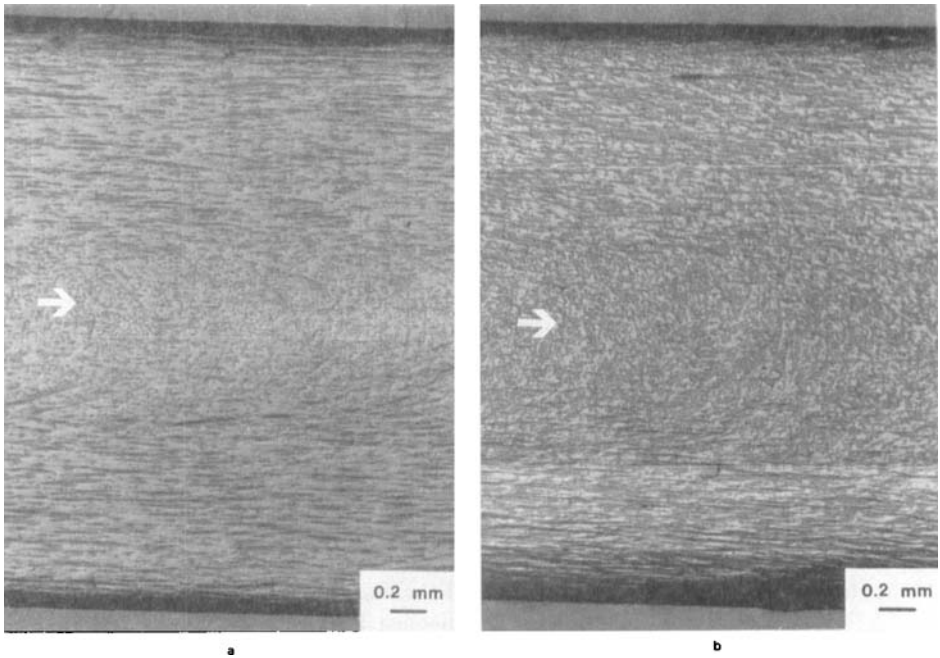

FIG. 2. Optical micrographs showing the orientation of glass fibers in a longitudinal cross section parallel to the mold-filling direction (MFD) (arrow): (a) 30 wt% composite, (b) 50 wt% composite; and in a transverse cross section perpendicular to the MFD: (c) 30 wt% composite, (d) 50 wt% composite.

the core macrolayer is created by the spreading radial flow. It is not clear whether, at high fiber loading, the orientation of the LCP resin is influenced by the surface of the glass fibers, which is an additional factor in carbon-fiber-reinforced LCP composites [38, 39]. It has been shown that the surface of the fibers can strongly influence the matrix morphology and the nature of the orientation in semicrystalline polymers [40]. Consequently, this type of directed crystallization, which is controlled by epitaxial phenomena at the interface, needs to be superimposed upon orientation effects due to the flow fields established during injection molding.

The importance of the effect of orientation on the fracture behavior is well demonstrated in Fig. 6. Here we see parabolic crack formation in the core,

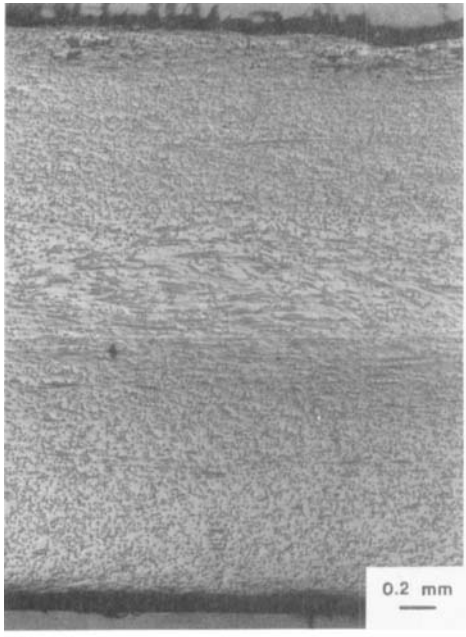

FIG. 2c

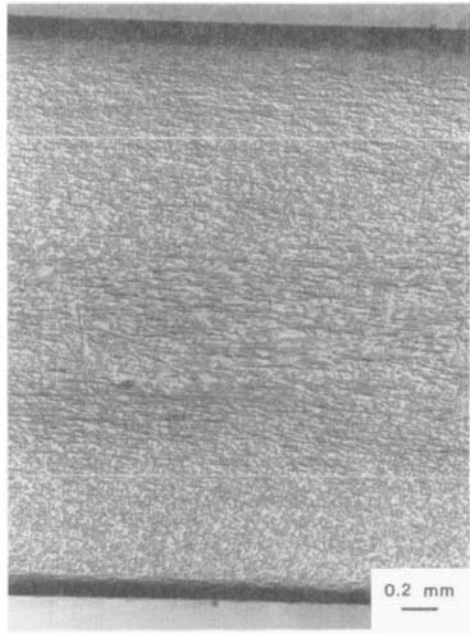

FIG. 2d

which occurred prior to ultimate failure during tensile deformation, indicating that the cracks presumably initiated and propagated along the weakest lines, which evidently are the flow lines in the core macrolayer. The occurrence of these cracks is a consequence of the difference in the orientation of the glass fibers in the skin and core macrolayers. Therefore, since the fibers in the core do not contribute to any mechanical enhancement by virtue of their orientation, the core starts to break at much lower stresses than the skin upon the application of unidirectional tensile stresses in the MFD. This behavior is well pronounced in $0°/90°$ laminate composites where the fibers are aligned perpendicular to each other in each ply [24].

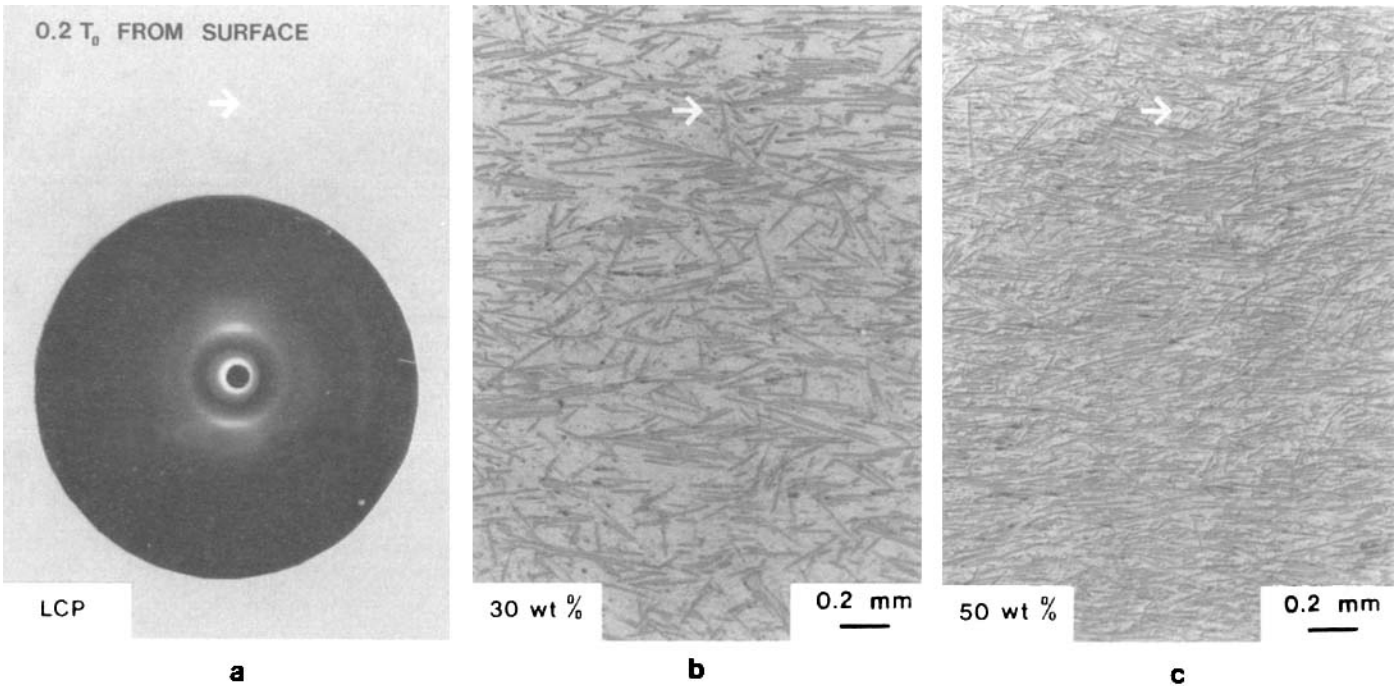

FIG. 3. In-plane cross sections at the surface showing (a) WAXS of the unreinforced LCP resin, (b) fiber orientation in the 30 wt% composite, and (c) in the 50 wt% composite.

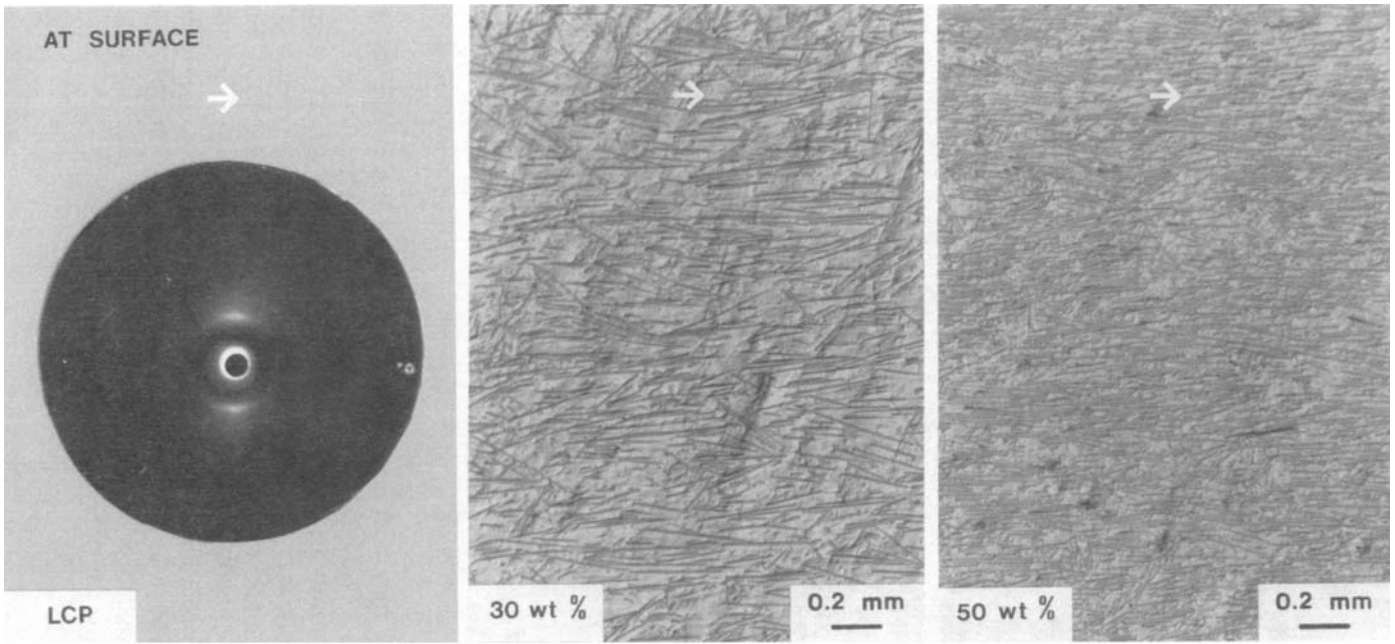

FIG. 4. In-plane cross sections 20% below the surface ($0.2t$) showing (a) WAXS of the unreinforced LCP resin, (b) fiber orientation in the 30 wt% composite, and (c) in the 50 wt% composite.

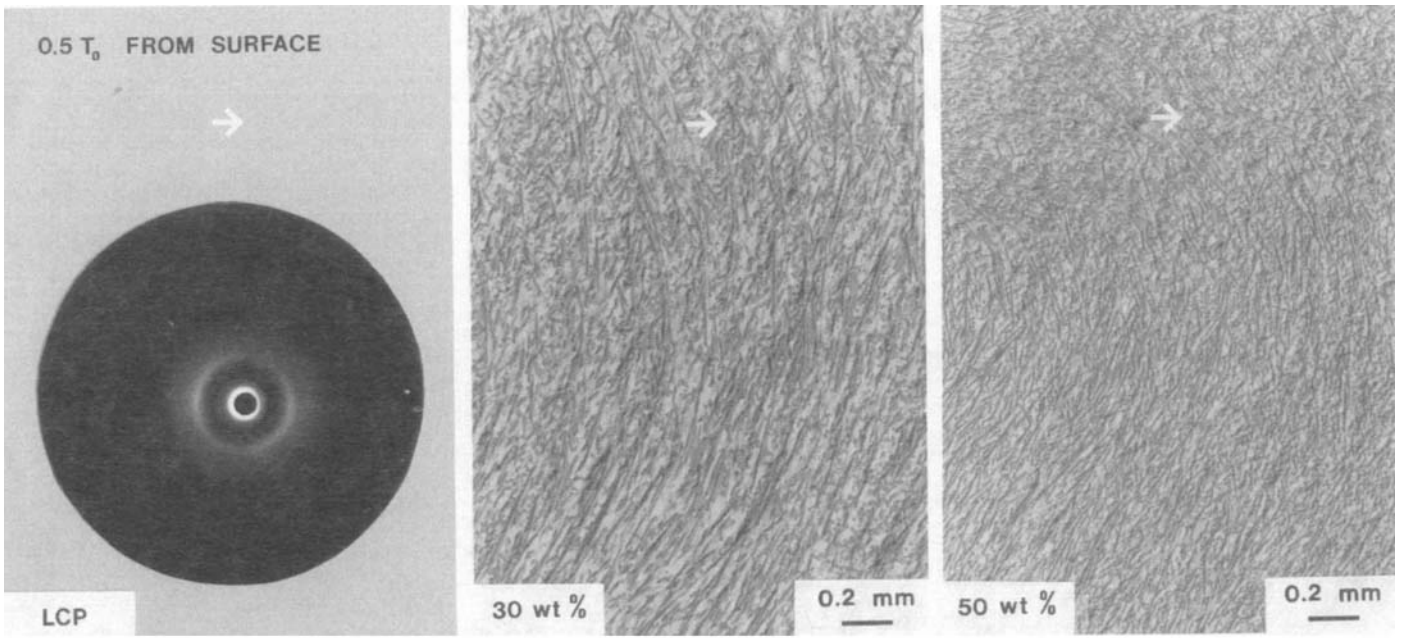

FIG. 5. In-plane cross sections at $0.5t$ showing (a) WAXS of the unreinforced LCP resin, (b) fiber orientation in the 30 wt% composite, and (c) in the 50 wt% composite.

Acoustic Emission in Tension

Typical acoustic emission AE signals monitored during uniaxial tensile deformation are shown in Fig. 7. The total number of AE events recorded in the composites is one order of magnitude higher than in the unreinforced LCP resin. While both composites displayed a progressive exponential increase in the number of AE events up to fracture, the unreinforced LCP resin showed a much less pronounced AE intensity before the failure point. In unreinforced LCP resin, the AE events, specifically at 2-4% strain, reflect fiber-related damage which seems to occur only at the surface of the material during tensile deformation. In a previous study [8] we reported the presence of a highly oriented fibrillar top layer on the surface. It is believed that most of the AE activities monitored correspond to the damage of this fibrillar top layer, as shall be further demonstrated later.

The corresponding amplitude distributions recorded during tension are given in Fig. 8. A clear difference in the shape of the distribution is evident. The amplitude distribution of the unreinforced LCP resin has a maximum in the 40-50 dB region, with relatively few events covering the whole range up to 99 dB, most events occurring between 2 and 4% strain. The amplitude distribution of the 30 wt% composite could be described as bimodal, with one low maximum at 40-55 dB and a second more predominant maximum in a relatively high-amplitude region between 55 and 70 dB. In addition, a very distinctive single peak occurs at 65 dB. This single peak and the maximum in the high-amplitude region between 55 and 70 dB are absent in the 50 wt% composite in which only a 40-50 dB maximum is observed.

In order to interpret these amplitude distributions and to correlate them with their source, two methods were employed. In the first method, samples were machined into various thicknesses, mainly into core and skin macrolayers, and tested in tension with simultaneous AE measurements. The corresponding amplitude distributions of the core and skin macrolayers of the LCP resin and its composites are given in Fig. 9. In the second method the amplitude distributions of the 30 and 50 wt% composites were divided into smaller sections based on different strain intervals up to the failure point, as shown in Figs. 10 and 11. The distribution breakdown was performed with a traveling optical microscope that monitored the deformation behavior.

From the amplitude distributions of the core and skin macrolayers of the unreinforced LCP resin (Fig. 9a), it is evident that the high-amplitude events emitted do not come from the core, but rather from the skin macrolayer. No events above 60 dB are detected in the core. Of the events emitted in the skin, 80-95% were indeed coming from the cracks that occur at the surface, as illustrated in Fig. 12. Side-view optical micrographs did not reveal any

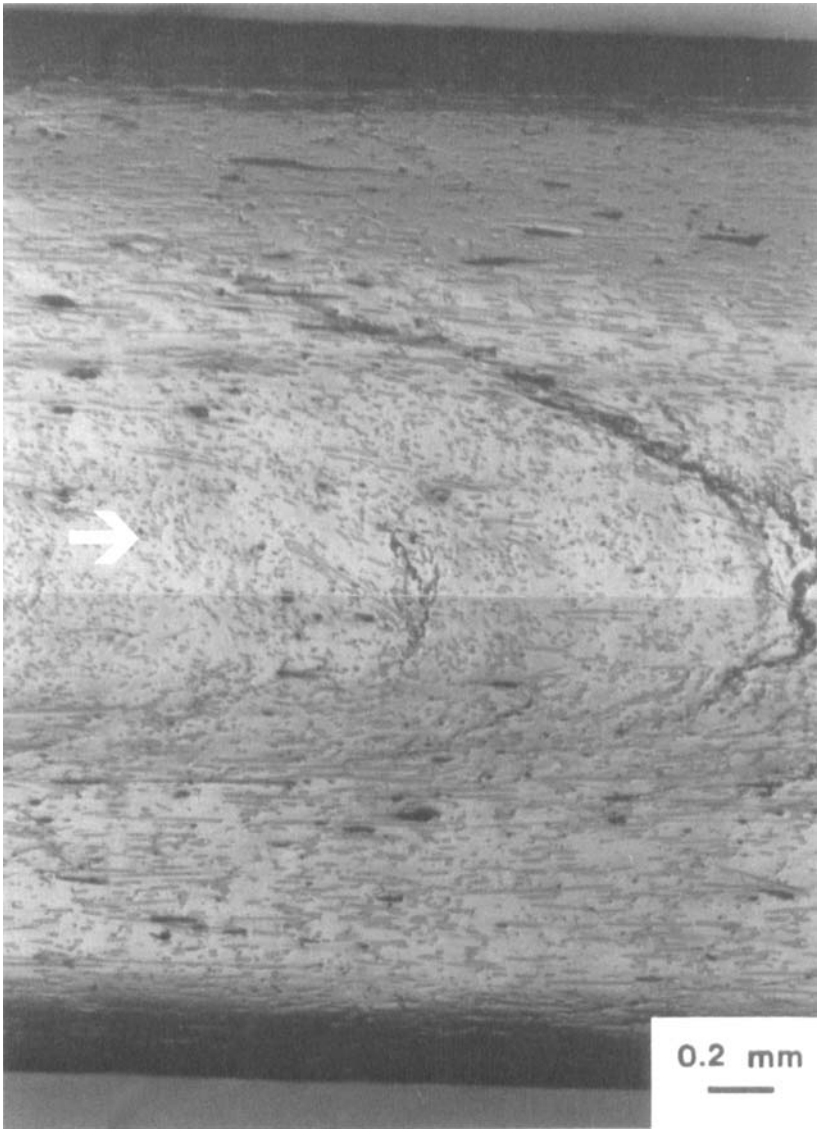

a

FIG. 6. Optical micrographs from a longitudinal cross section parallel to the MFD showing parabolic cracks occurring in the core during tensile deformation of (a) the 30 wt% composite and (b) the 50 wt% composite.

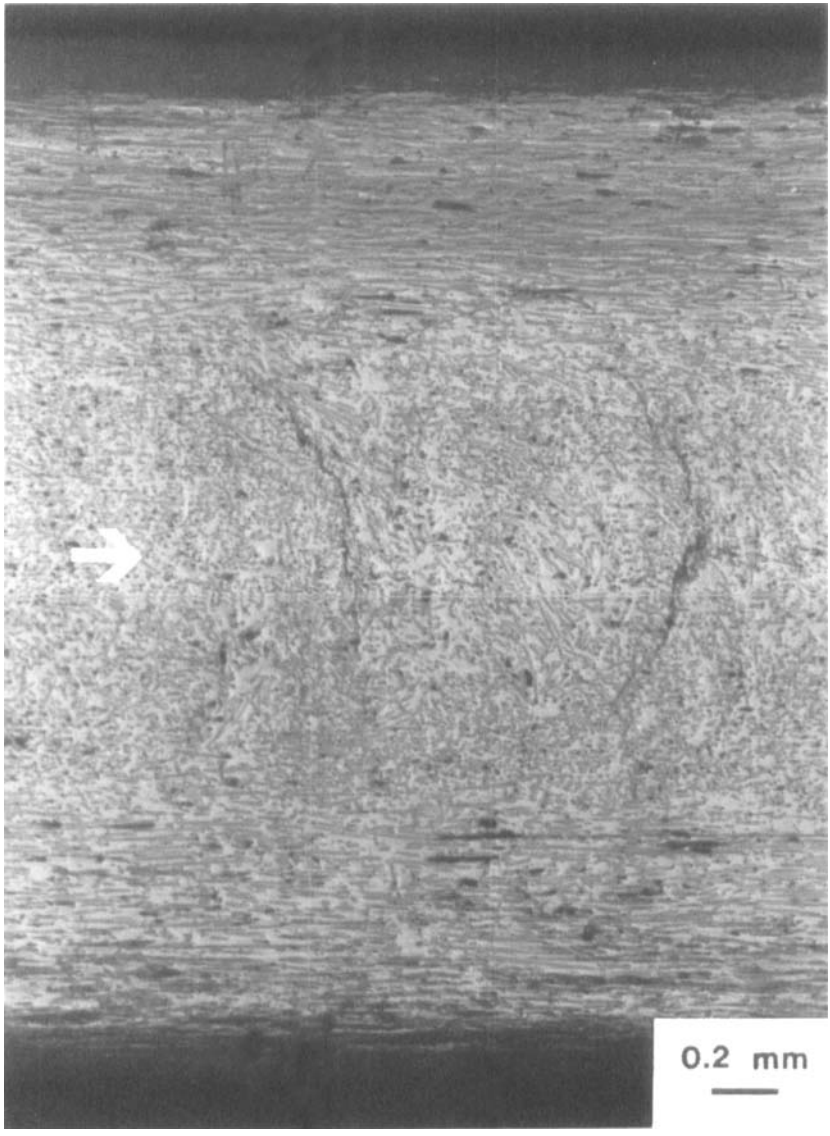

b

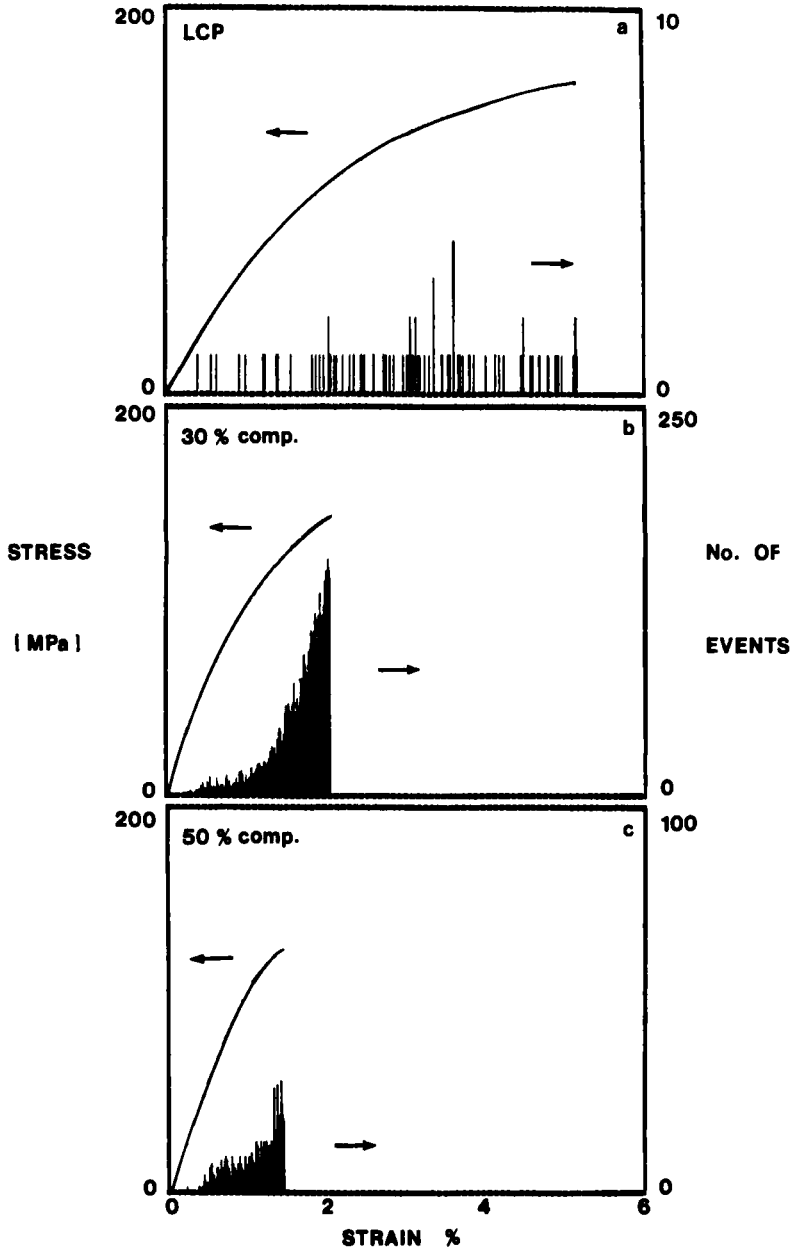

FIG. 7. Acoustic emission AE events monitored during tensile deformatior of (a) the unreinforced LCP resin, (b) the 30 wt% composite, and (c) the 50 wt% composite.

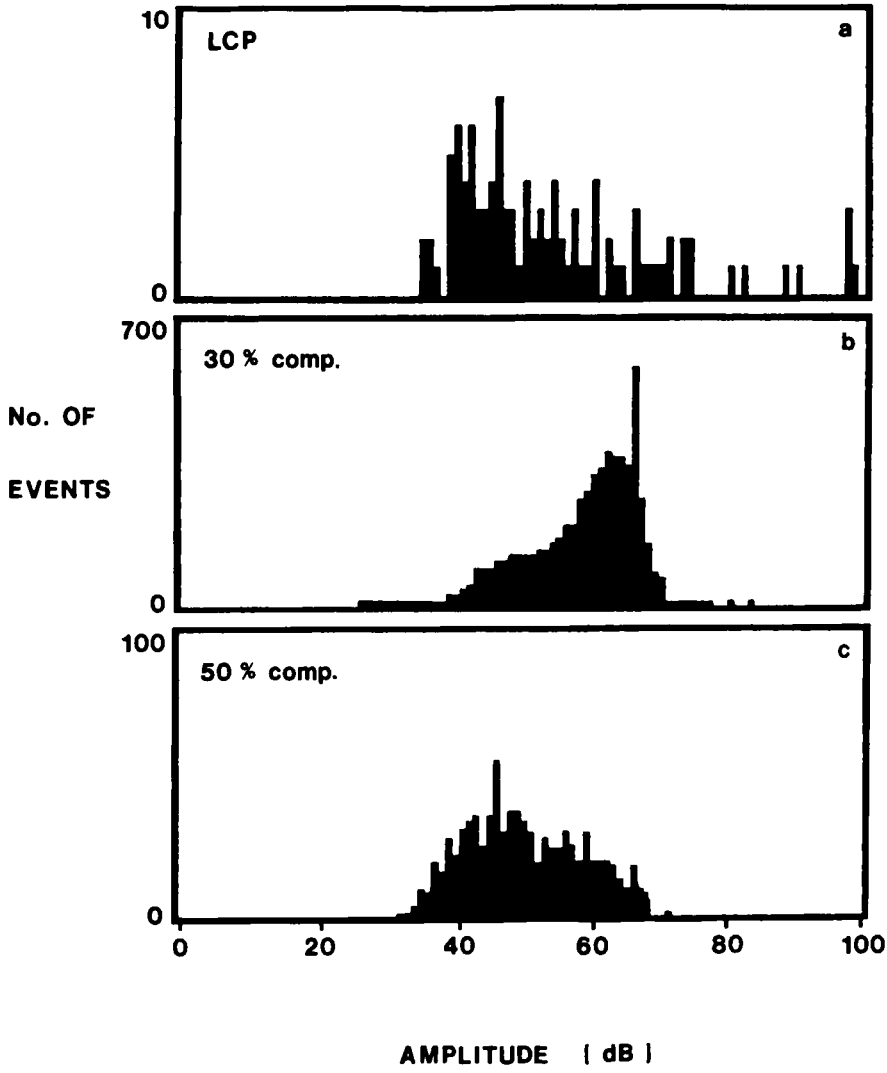

FIG. 8. The corresponding amplitude distributions of (a) the unreinforced LCP resin, (b) the 30 wt% composite, and (c) the 50 wt% composite.

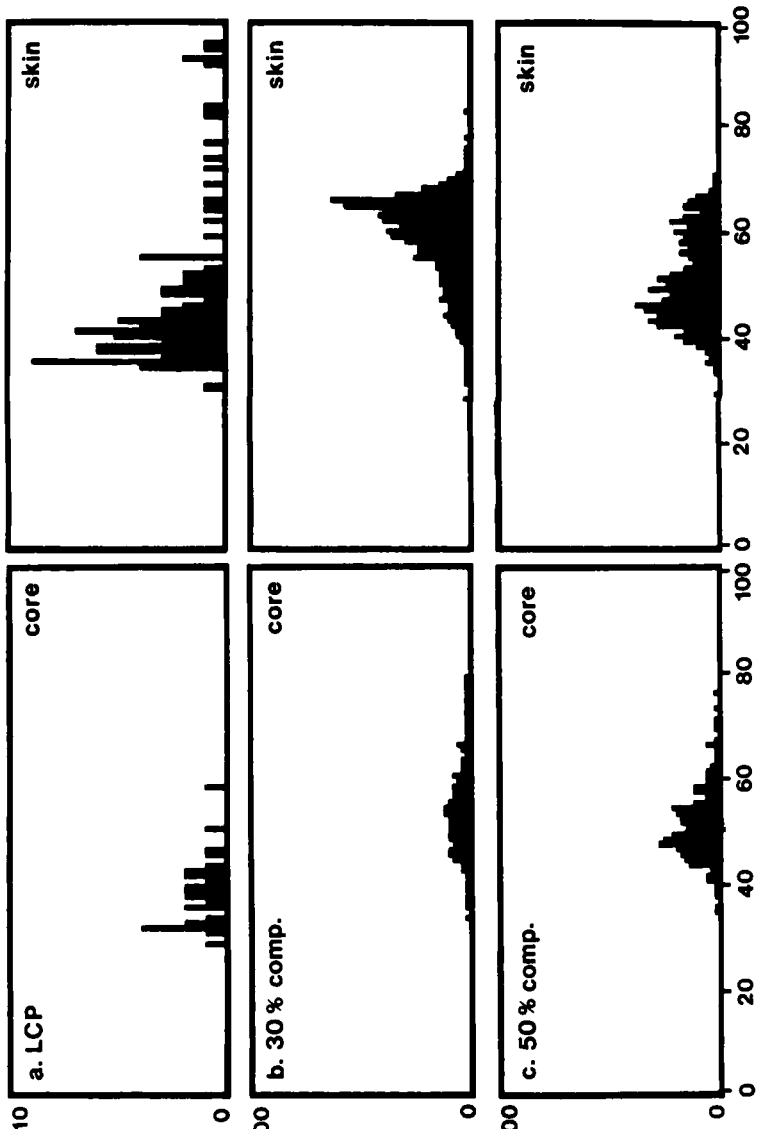

FIG. 9. Comparison between the amplitude distributions of the core and skin macrolayers of (a) the unreinforced LCP resin, (b) the 30 wt% composite, and (c) the 50 wt% composite.

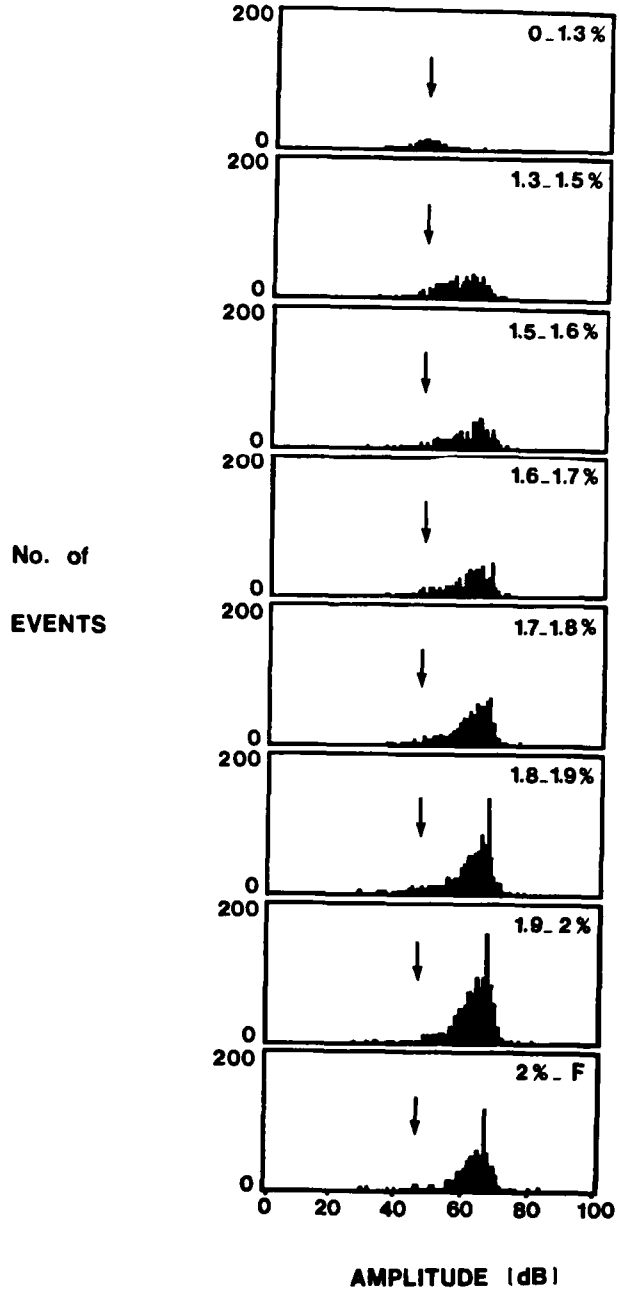

FIG. 10. Amplitude distributions of the 30 wt% composite recorded at different strain intervals to fracture. The arrows indicate the location of the maximum at 0-1.3% strain.

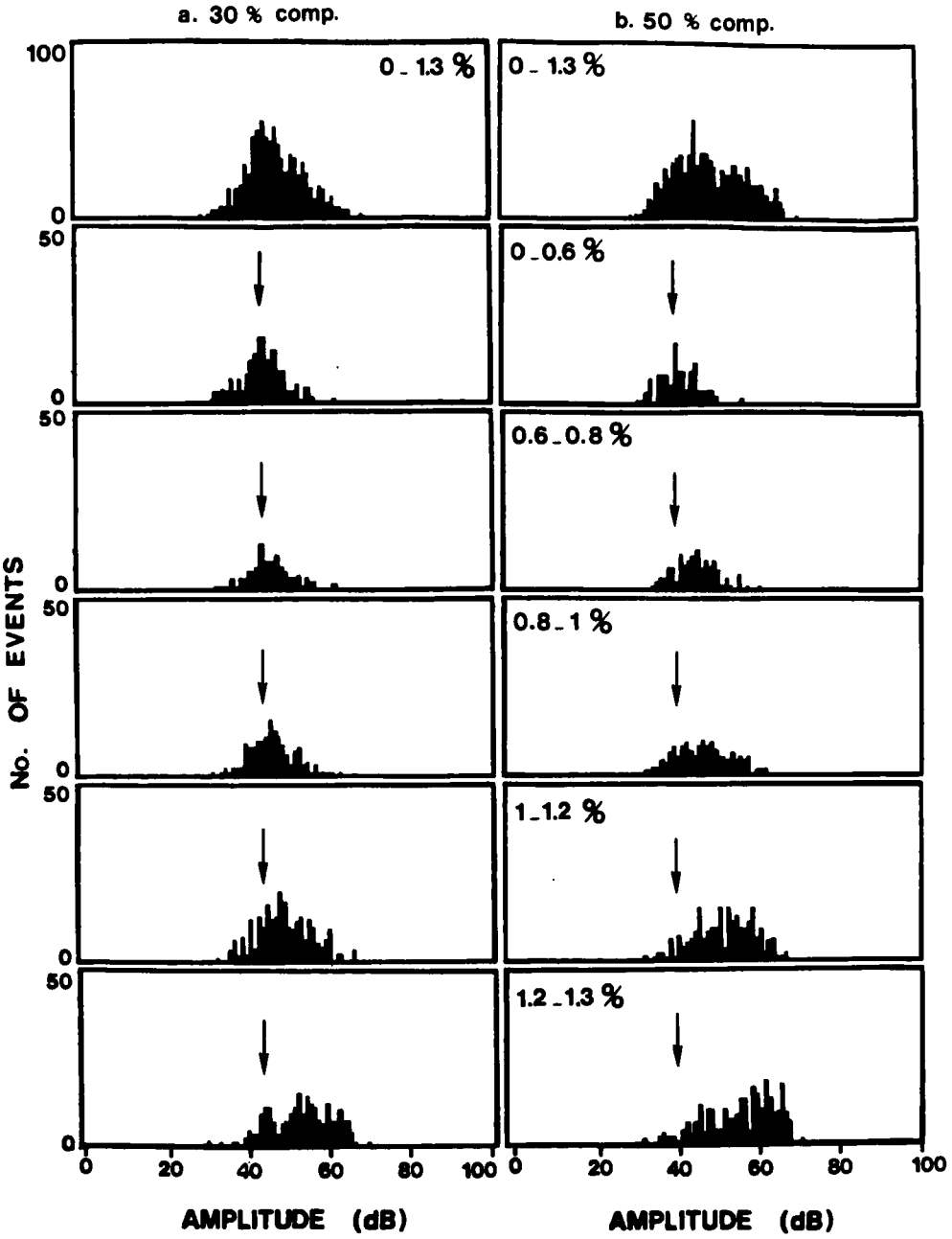

FIG. 11. Comparison between the amplitude distributions of (a) the 30 wt% composite and (b) the 50 wt% composite at strain intervals up to 1.3% strain.

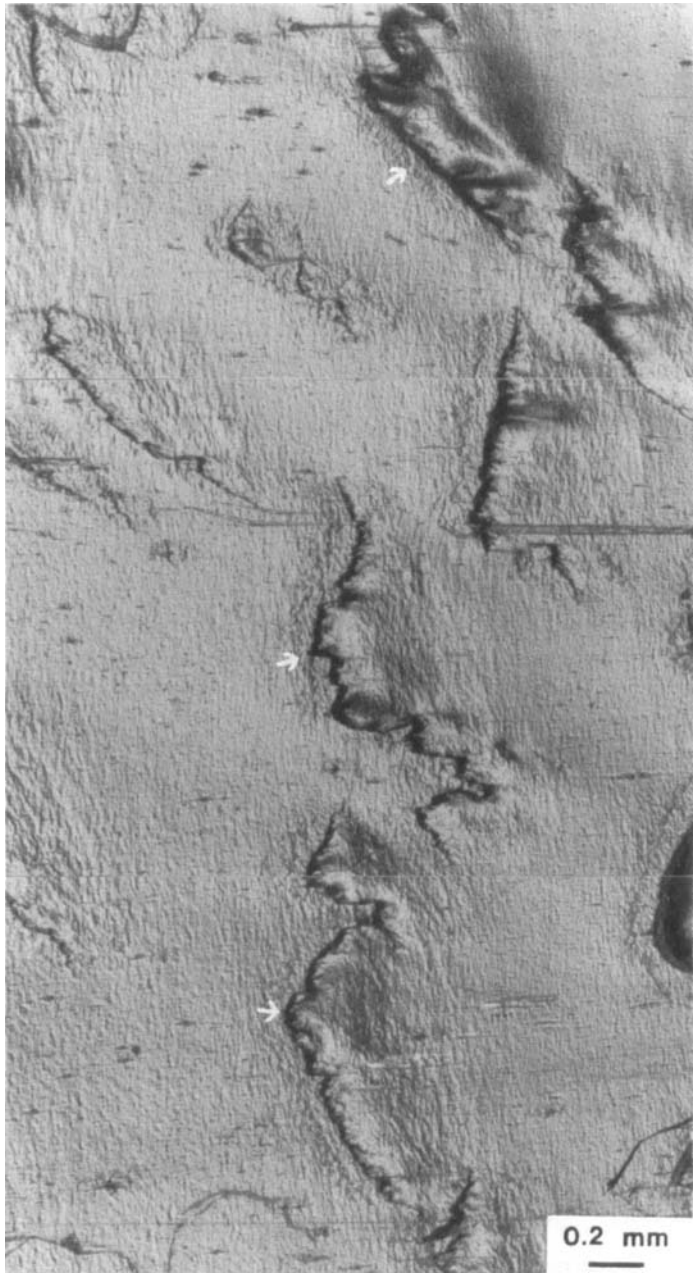

FIG. 12. Optical micrograph showing the surface cracks (see arrows) occurring in the so-called "top layer" of the skin in the unreinforced LCP resin during tensile deformation.

type of apparent damage or fracture. Furthermore, if only the top surface is machined, all of the high-amplitude events disappear (not shown). Consequently, one can conclude that the high-amplitude events recorded above 70-75 dB in the LCP resin originate from the surface of the sample. They indeed reflect the damage associated with the fibrillar top layer which usually occurs between 2 and 4% strain.

The amplitude distributions for the core and skin macrolayers of the composites are given in Figs. 9(b) and 9(c). For the 30 wt% composite, most of the events in the core are distributed in the low-amplitude region, with very few events above 65 dB, whereas in the skin the distribution is weighted toward the high region, including the distinctive peak at 65 dB. The distribution in the skin is quite similar to the composite itself (Fig. 8b). Therefore, the core macrolayer seems to be associated mainly with the low-amplitude events and, conversely, the skin macrolayer with the high-amplitude events. In the 50 wt% composite, no significant difference between the distributions of the core and skin is observed although the skin has a slightly higher peak between 55 and 70 dB.

The second method consisted of dividing the amplitude distribution of both composites into smaller sections (Figs. 10 and 11). For the 30 wt% composite, up to approximately 1.3% strain, most of the events occur in the low-amplitude region between 40-50 dB. These low-amplitude events represent nearly 15% of the total. As the strain is increased, a gradual continuous shift in the maximum toward higher amplitude values occurs. The distinctive peak at 65 dB starts to appear at nearly 1.7% strain. More events are recorded in the high-amplitude region, 55-70 dB, and conversely less in the low-amplitude region, below 50 dB. The number of events occurring in the last 0.2% strain constitutes approximately half the total. This gradual shift in the amplitude distribution from low to higher values implies that damage originates in the core macrolayer followed by the skin. This conclusion is supported by the sumultaneous optical micrographs taken at different strain levels from a side view of the sample during the tension test. Small cracks were observed to originate in the core macrolayer in the range of 1.3% strain. The cracks, which grew further into larger parabolic shapes, are visible in Fig. 6(a). No apparent damage was detected in the skin macrolayer when observed from either the side or the front view of the sample. Therefore, one can conclude that the core fails prior to the skin macrolayer. The initiation of cracks in the core gives rise to the low-amplitude distribution between 40-50 dB. The growth of these parabolic cracks further induces severe damage in the skin macrolayer by stress transfer, resulting into a gradual shift in the AE amplitude distribution toward higher values between 55-70 dB.

In the 50 wt% composite, similar cracks are observed in the core macrolayer with no apparent damage in the skin, as shown in Fig. 6(b). Consequently, no difference in the amplitude distribution of the core of both composites is expected, as shown in Figs. 9(b) and 9(c). The main difference between the two composites lies in the skin macrolayer. It is evident that the predominant peak at 55-70 dB in the 30 wt% composite is almost absent in the 50 wt% composite. This strongly suggests that some energy absorption mechanisms operating in the skin of the 30 wt% composite no longer exist in the 50% composite, which would explain its premature failure. These mechanisms, as well as the reason for the premature failure of the 50 wt% composite, will be discussed relative to SEM examination of fracture surfaces in the next section.

If both composites are compared up to 1.3% strain, a typical fracture strain of the 50 wt% composite, similar amplitude distributions are observed, as demonstrated in Figs. 11(a) and 11(b). Both composites exhibit similar distributions with respect to the shape and number of events. The main difference is that the skin macrolayer of the 30 wt% composite continued to carry the load following cracking of the core, while the 50 wt% composite failed prematurely at 1.3% strain.

SEM Fracture Surfaces

SEM fracture surface studies reveal similar types of microdamage in the core macrolayer of both composites but differences in the skin macrolayer. In the core, as shown in Figs. 13(a) and 13(c), only transverse fiber pull-out and transverse matrix cracking or deformation could be observed. Little or no fiber breakage could be seen. These two types of damage are believed to give rise to the same low amplitude distributions presented in Figs. 9(b) and 9(c) for the core of the composites. This conclusion is also supported by the simultaneous OM pictures taken during the deformation, which showed only cracking of the core macrolayer (Figs. 6a and 6b).

A difference in the fracture surfaces between both composites is clearly observed in the skin macrolayer. This difference is also manifested in their amplitude distributions (Fig. 9) as discussed earlier. In the 30 wt% composite case (Fig. 13b), three main types of microdamage could be detected, namely: fiber breakage, fiber pull-out, and matrix deformation. Contrary to the core, the matrix in the skin is preferentially oriented along the MFD, as has been demonstrated from the WAXS in Fig. 3. Although no direct simultaneous microscopic observations with the AE data could be obtained for the skin macrolayer, these three types of microdamage are believed to be responsible for the high-amplitude distribution between 55-70 dB (Fig. 9b), which was

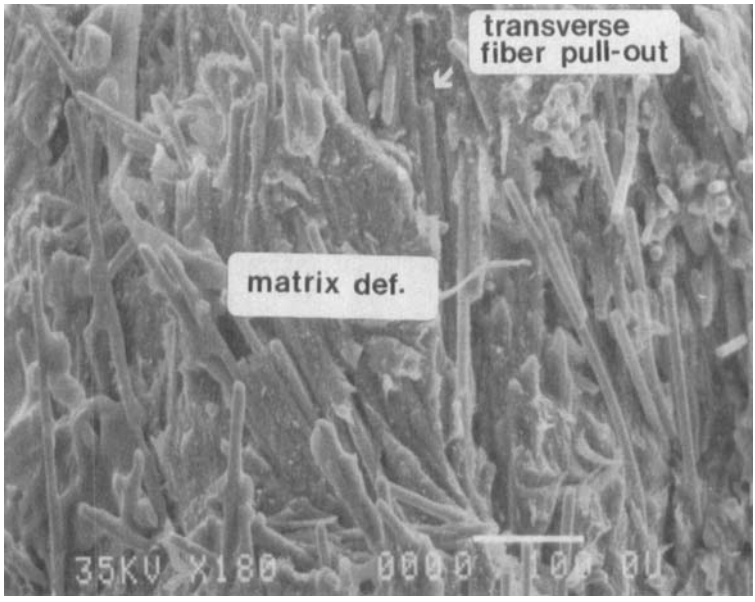

a. core ; 30 %

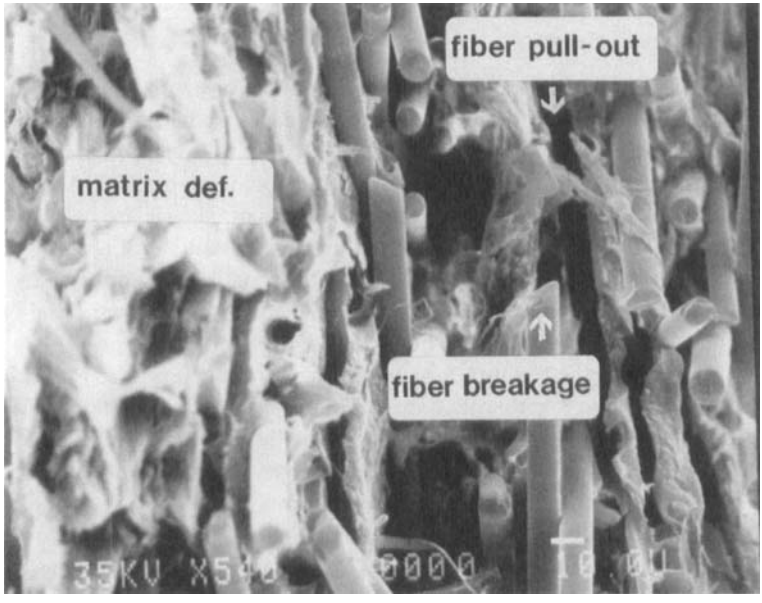

b. skin ; 30%

FIG. 13. Scanning electron micrographs of fracture surfaces: (a) the core of the 30 wt% composite and (b) the skin, and similarly, (c) the core of the 50 wt% composite and (d) the skin. The MFD is perpendicular to the plane of the micrographs.

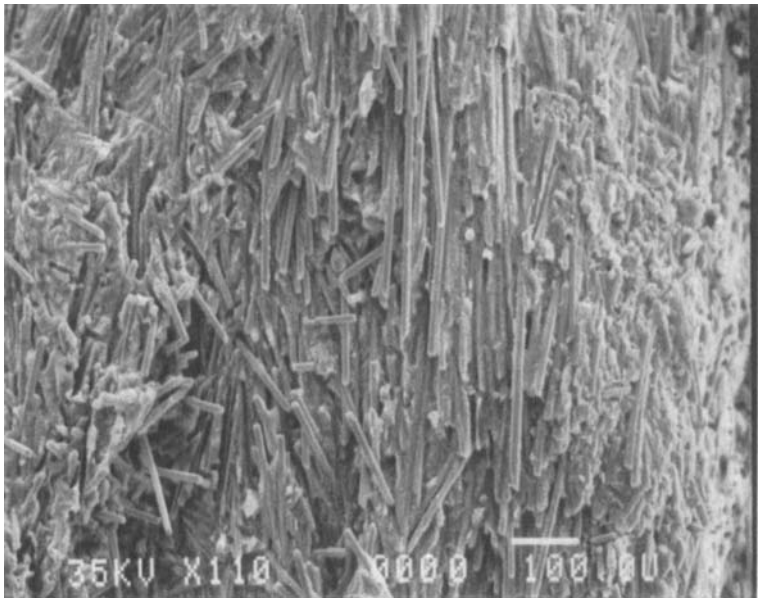

c. core ; 50%

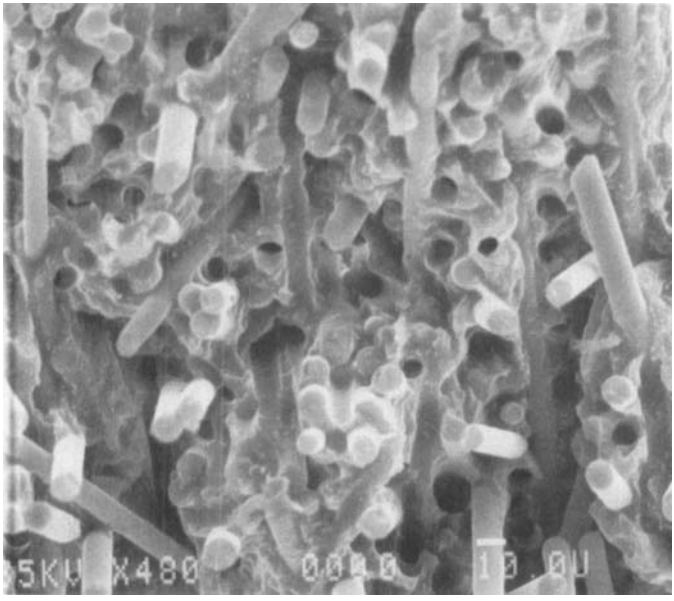

d. skin ; 50%

found to develop in the latter stages of the deformation (Fig. 10). The sequence of these types of microdamage will be described in the next section. In the 50 wt% composite, the fracture surface could be described as more brittle with little or less resin material than in the 30 wt% composite, as shown in Fig. 13(d). Consequently, one sees fiber breakage, more fiber pull-out, and almost no matrix deformation. Therefore, the absence of the 55-70 dB peak in the skin macrolayer of the 50 wt% composite (Fig. 9c) could be attributed to inadequate fiber/matrix interactions due to insufficient resin material available to surround the fibers effectively. This could also explain why this composite fails prematurely.

Microfailure Mechanisms

SEM was used to examine in detail the microdeformation processes in the skin macrolayer of both composites. The technique employed, which consisted of bending a sample in a mini 3-point bending device *in situ* in the SEM, has been described elsewhere [25]. The as-polished surface of a 30 wt% composite specimen is shown in Fig. 14(a). No damage is observed on the surface as a result of polishing. As the stress level was increased, fracture first occurred in the glass fibers and to a lesser extent at the fiber ends (Fig. 14b). Due to breakage of the conducting coating and the generation of electrostatic charges in the SEM chamber, these fractured sites appear brighter than the undamaged areas on the surface. As bending was increased, cracks along fiber sides or interfacial debonding took place (Fig. 14c), followed shortly by formation of microcracks in the matrix and growth of cracks into the matrix from the fiber ends (Fig. 14d). Interfacial debonding led to fiber pull-out (Fig. 14e). Finally, as the stress level was further increased, interconnection of matrix cracks (Fig. 14f) produced catastrophic failure (Fig. 14g).

The above failure mechanisms were also found in the 50 wt% composite, except that much less pronounced or almost no matrix cracks were seen. This was attributed to a deficiency in the amount of resin material available with respect to the high fiber loading, as was discussed before. For the 50 wt% composite, fiber breakage and fiber-end cracks are shown in Fig. 15(a). Figure 15(b) depicts interfacial debonding and fiber pull-out, while catastrophic failure is seen in Fig. 15(c).

It is evident that the microdeformation processes examined in both composites are numerous and could overlap, which makes the task of assigning the AE amplitudes more difficult. It was mentioned earlier that a number of authors have correlated high-amplitude events with fiber breakage, intermediate values with interfacial debonding, and low-amplitude events with

matrix cracking. Others have concluded that matrix cracking and/or fiber breakage could give rise to the high-amplitude events. This study has suggested that the low-amplitude events in the LCP composite systems correspond mainly to transverse fiber pull-out and transverse matrix cracking in the core macrolayer, while the high-amplitude events correspond to cooperative phenomena involving fiber breakage, fiber pull-out, and matrix deformation in the skin macrolayer. Not enough evidence is available to assign confidently the exact amplitude distribution for each of the individual microdeformation processes delineated by the 3-point bend test. However, the distinctive peak at 65 dB observed during tension could be correlated with the fiber breakage process. This is based on the assumption that glass fibers are the only structural elements in the composite which have a uniform geometrical cross section and hence, upon fracture, they should emit signals of similar amplitudes. Few events at 65 dB could be seen in the earlier stages of the deformation (Fig. 10). On the other hand, fiber debonding and pull-out are presumably the reasons behind the dominant 55-70 dB peak in the skin macrolayer of the 30 wt% composite.

CONCLUSIONS

1. The average orientation of glass fibers in the injection-molded LCP composites was similar to the preferred molecular orientation in the unreinforced LCP resin. Most of the fibers in the skin macrolayer of both composites were oriented in the mold-filling direction, whereas the fibers in the core were partially aligned perpendicular to the mold-filling direction.

2. The core of the 30 wt% composite fractured prior to the skin structure. Two major AE amplitude distributions were observed: a low distribution at 40-55 dB, which corresponds to fracture of the matrix material, and transverse fiber pull-out in the core macrolayer. A more intense, high-amplitude distribution, which occurred between 55 and 70 dB, reflects complex cooperative phenomena involving fiber breakage, debonding, pull-out, and matrix deformation in the skin structure. The sequence of these microdamage processes was elucidated by a 3-point bend test in the SEM.

3. The 50 wt% composite exhibited only a low-amplitude distribution at 40-50 dB. Growth of parabolic cracks, similar to those in the 30 wt% composite, was the main failure mode occurring in the core macrolayer, which also corresponds to matrix cracking and transverse fiber pull-out. The premature failure of this composite was attributed to inadequate fiber/matrix interactions in the skin macrolayer due to insufficient resin surrounding the

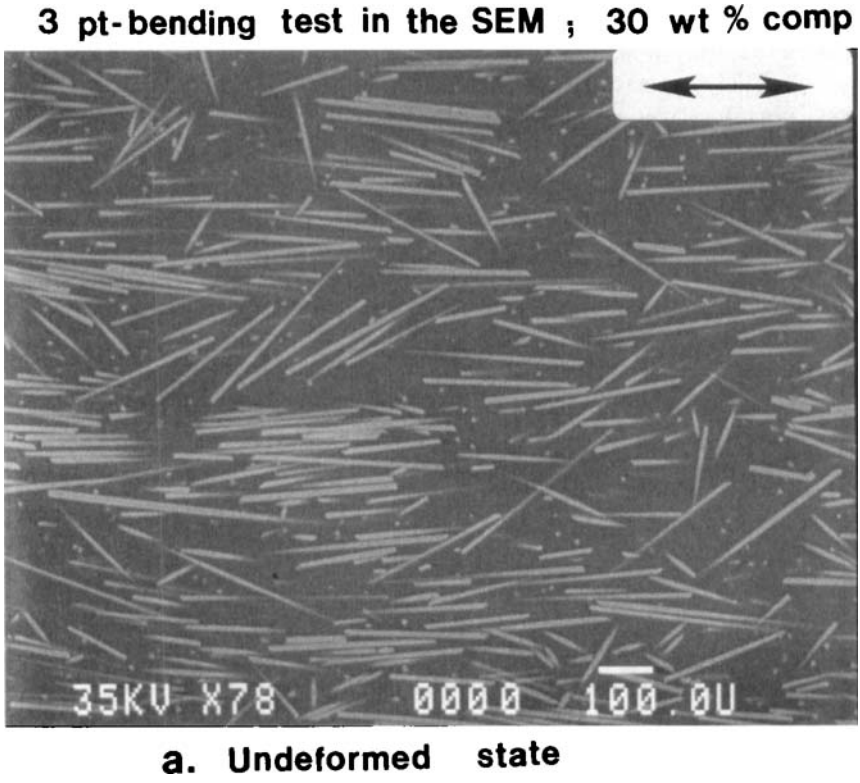

FIG. 14. Scanning electron micrographs of the 30 wt% composite during the three-point-bend test in the SEM showing the localized failure sequence. MFD and direction of bending indicated by arrows.

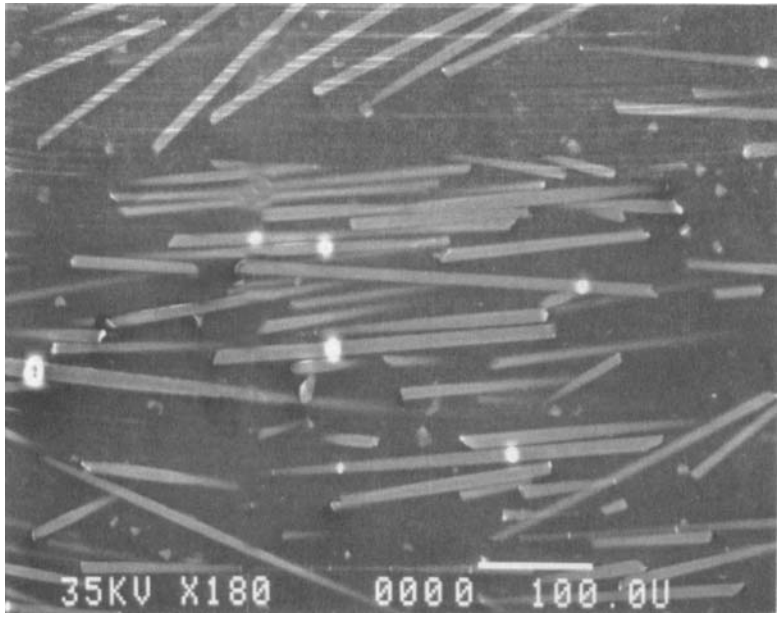

b. Fiber breakage + small fiber-end cracks

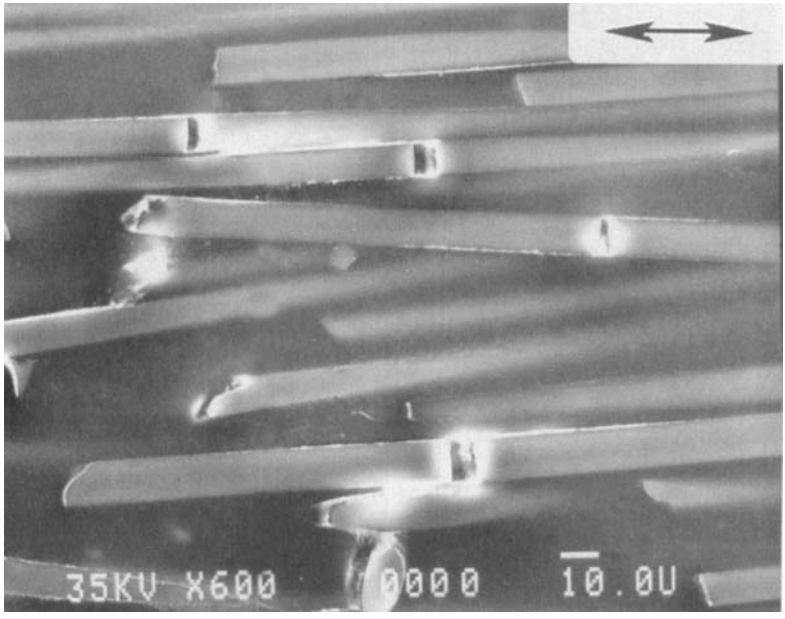

c. Interfacial debonding

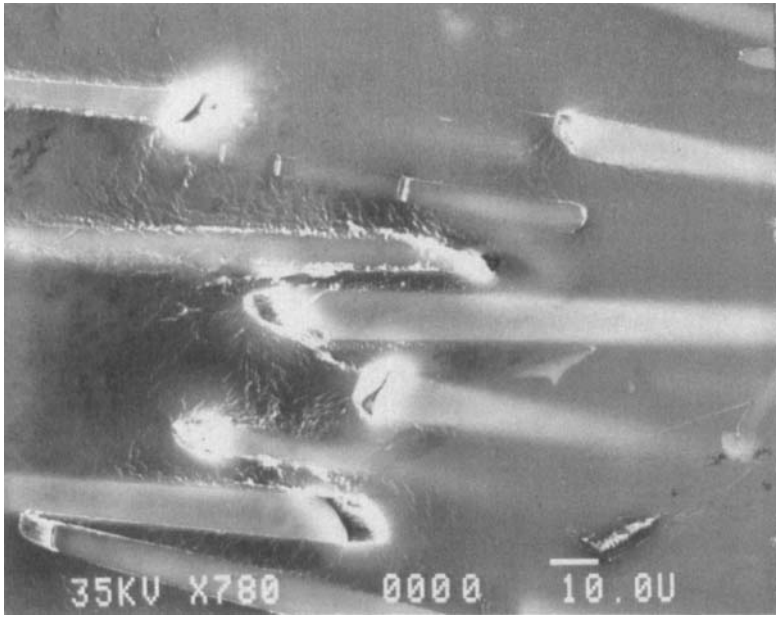

d. Local cracks + large fiber-end cracks

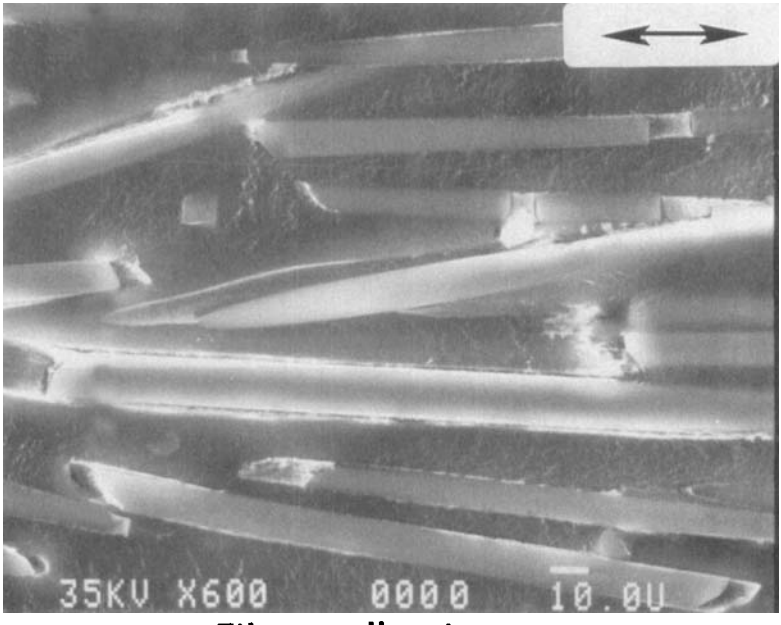

e. Fiber pull-out

f. Interconnection of local & fiber-end cracks

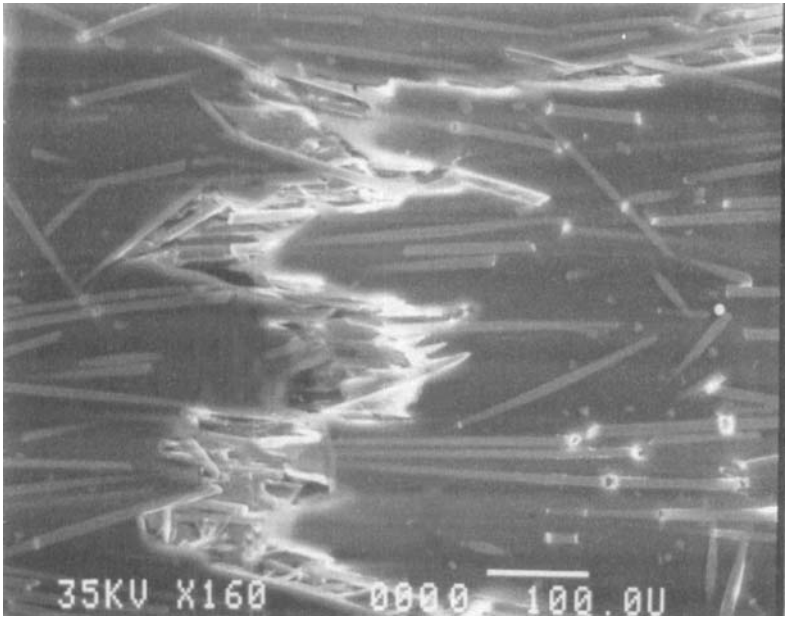

g. Catastrophic failure

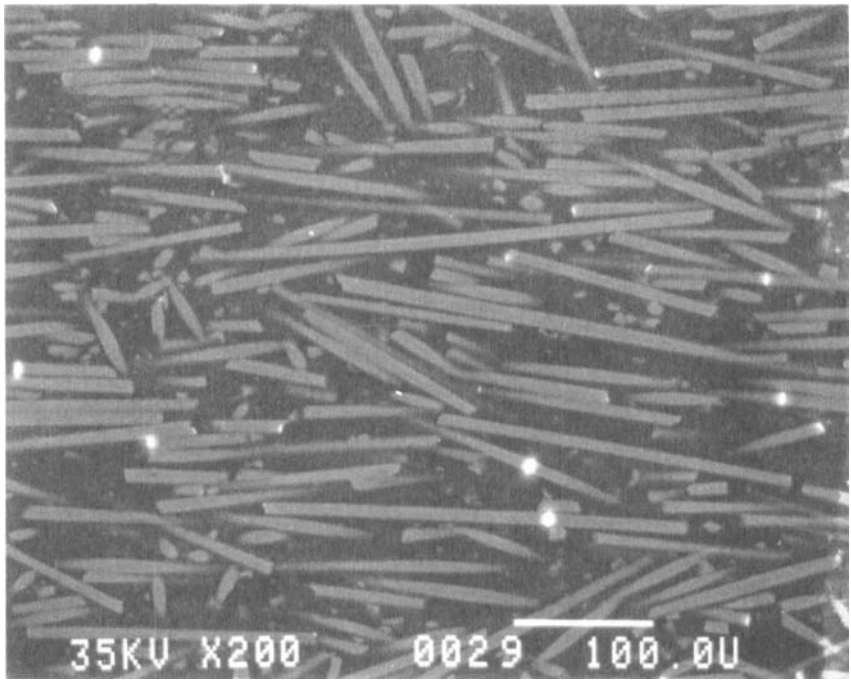

a

FIG. 15. Scanning electron micrographs of the 50 wt% composite during the three-point bend test in the SEM showing the localized failure sequence. (a) Fiber breakage and fiber-end cracks, (b) interfacial debonding and few fiber pull-out, (c) catastrophic failure.

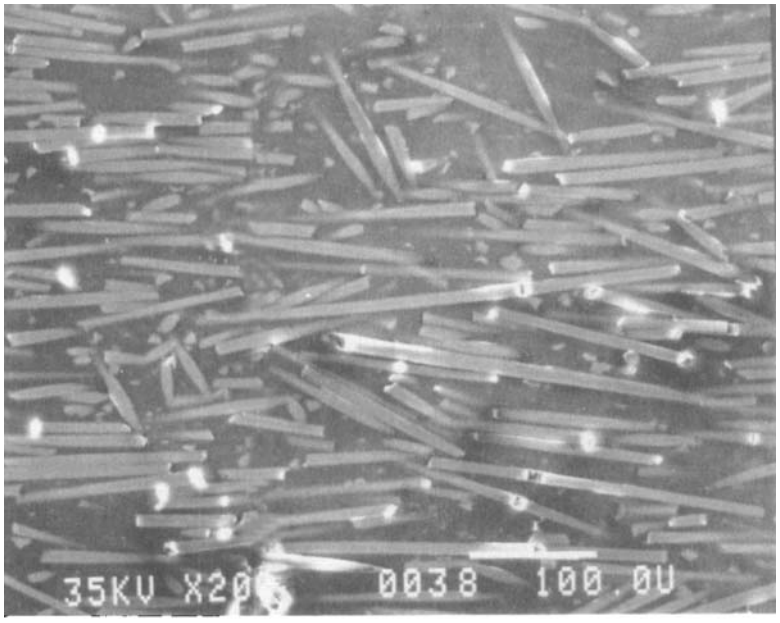

b

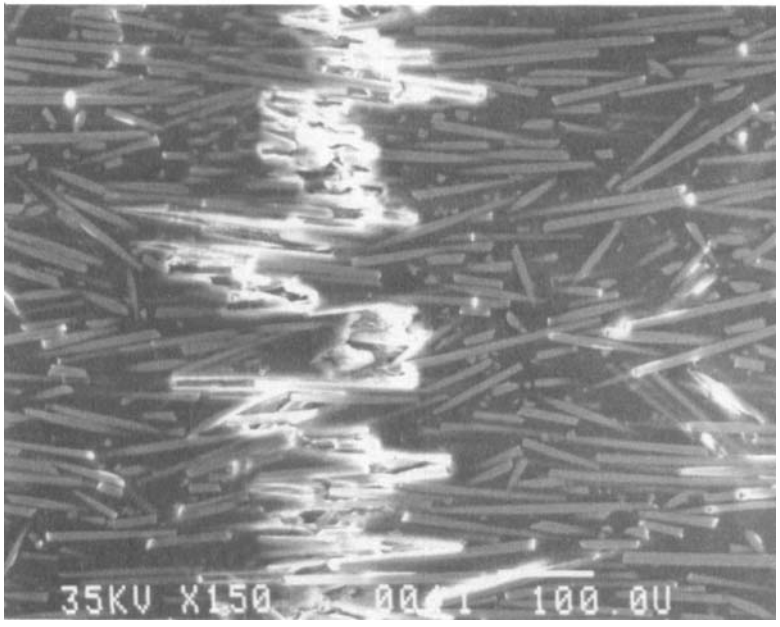

c

fibers for effective reinforcement. This led to a brittle type of fracture, with no high AE amplitude events.

ACKNOWLEDGMENTS

The authors gratefully acknowledge the generous financial support of the U.S. Army Research Office (Grant No. DAAG 29-84-K-0155) and the Celanese Corporation for providing the samples.

REFERENCES

[1] M. J. Folkes, *Short Fiber Reinforced Thermoplastics,* Research Studies Press, Chichester, 1982.
[2] G. Calundann and M. Jaffe, in *Proceedings of The Robert A. Welch Conferences on Chemical Research, 26th, Synthetic Polymers, Houston, Texas, 15 to 17 November 1982,* R. A. Welch Foundation, Houston, 1983, p. 247.
[3] W. J. Jackson and H. F. Kuhfuss, *J. Polym. Sci., Polym. Chem. Ed., 14,* 2043 (1976).
[4] F. E. McFarlane, V. A. Nicely, and T. G. Davis, in *Contemporary Topics in Polymer Science,* Vol. 2 (E. M. Pearce and J. R. Schaefgen, eds.), Plenum, New York, 1977, p. 109.
[5] Z. Ophir and Y. Ide, *Polym. Eng. Sci., 23,* 792 (1983).
[6] E. G. Joseph, G. L. Wilkes, and D. G. Baird, *Ibid., 25,* 377 (1985).
[7] H. Thapar and M. Bevis, *J. Mater. Sci. Lett., 2,* 733 (1983).
[8] T. Weng, A. Hiltner, and E. Baer, *J. Mater. Sci., 21,* 744 (1986).
[9] L. C. Sawyer and M. Jaffe, *Ibid., 21,* 1897 (1986).
[10] D. G. Baird and G. L. Wilkes, *Polym. Eng. Sci., 23,* 632 (1983).
[11] H. Voss and K. Friedrich, *J. Mater. Sci., 21,* 2889 (1986).
[12] J. H. Williams and S. S. Lee, *J. Compos. Mater., 12,* 348 (1978).
[13] R. L. Mehan and J. V. Mullin, *Ibid., 5,* 266 (1971).
[14] T. J. Fowler, *Acoustic Emission Testing of Fiber Reinforced Plastics,* Paper presented at ASCE Fall Convention, San Francisco, 1980.
[15] T. S. Brown and J. Mitchell, Paper Presented at the 35th Reinforced Plastics/Composites International Conference, New Orleans, Louisiana, 5-8 February 1980, Paper No. 26-B.
[16] H. Otsuka and H. A. Scarton, *J. Compos. Mater., 15,* 591 (1981).
[17] D. Short and J. Summerscales, *Composites, 15,* 200 (1984).

[18] J. Wadin and A. A. Pollock, Paper Presented at the 9th National Technical Conference SAMPE, Atlanta, Georgia, October 1977, p. 519.
[19] J. J. Ryder and J. Wadin, PaperPresented at ASNT National Spring Conference, San Diego, California, April 2-5, 1979, p. 9.
[20] J. Wolters, *J. Acous. Emiss., 3,* 51 (1984).
[21] M. R. Gorman and T. H. Ryting, First ICARP, SPI, San Francisco, California, July 19-20, 1983.
[22] J. F. Mandell and B. L. Lee, in *Composite Materials: Testing and Design, 6th Conference* (I. M. Daniel, ed.), American Society for Testing and Materials, 1982, p. 200.
[23] N. Sato, T. Kurauchi, S. Sato, and O. Kamigaito, *J. Mater. Sci., 19,* 1145 (1984).
[24] F. J. Guild, M. G. Phillips, and B. Harris, *Non-Destr. Test. Int.,* p. 209 (October 1980).
[25] N. Sato, T. Kurauchi, S. Sato, and O. Kamigaito, *J. Mater. Sci. Lett., 2,* 188 (1983).
[26] L. A. Goettler, *Polym. Compos., 5,* 60 (1984).
[27] R. B. Pipes, R. L. McCullough, and D. G. Taggart, *Ibid., 3,* 34 (1982).
[28] M. W. Darlington, P. L. McGinley, and G. R. Smith, *J. Mater. Sci., 11,* 877 (1976).
[29] P. F. Bright, R. J. Crowson, and M. J. Folkes, *Ibid., 13,* 2497 (1978).
[30] M. J. Folkes and D. A. M. Russell, *Polymer, 21,* 1252 (1980).
[31] K. Friedrich, *Compos. Sci. Technol., 22,* 43 (1985).
[32] C. Lhymn and J. M. Schultz, *J. Mater. Sci. Lett., 4,* 1244 (1985).
[33] G. Kalishe and H. Seifert, *Plaste Kautsch., 22,* 837 (1973).
[34] Z. Tadmor, *J. Appl. Polym. Sci., 18,* 1753 (1974).
[35] K. N. Murty and G. F. Molden, *Polym. Eng. Sci., 17,* 848 (1977).
[36] R. J. Crowson, M. J. Folkes, and P. F. Bright, *Polym. Eng. Sci., 20,* 925 (1980).
[37] S. Kenig, *Polym. Compos., 7,* 50 (1986).
[38] T. S. Chung, NASA Report No. CR-172323, National Aeronautics and Space Administration, Langley Research Center, Hampton, Virginia 23665, May 1984.
[39] T. S. Chung, Z. Gurion, and J. B. Stamatoff, *Polym. Compos., 6,* 181 (1985).
[40] J. Bessell and J. B. Shortall, *J. Mater. Sci., 10,* 2035 (1975).